Towards a solution of the Γ_n/Γ_p puzzle in the nonmesonic weak decay of Λ hypernuclei

G. Garbarino,[1,2] A. Parreño,[1] and A. Ramos[1]
[1]*Departament d'Estructura i Constituents de la Matèria, Universitat de Barcelona, E-08028 Barcelona, Spain*
[2]*Dipartimento di Fisica Teorica, Università di Torino and INFN, Sezione di Torino, I–10125 Torino, Italy*
(Received 20 November 2003; published 10 May 2004)

One of the main open problems in the physics of Λ hypernuclei is the lack of a sound theoretical interpretation of the large experimental values for the ratio $\Gamma_n/\Gamma_p \equiv \Gamma(\Lambda n \to nn)/\Gamma(\Lambda p \to np)$. To approach the problem, we have incorporated a one-meson-exchange model for the $\Lambda N \to nN$ transition in finite nuclei in an intranuclear cascade code for the calculation of single- and double-coincidence nucleon distributions corresponding to the nonmesonic weak decay of $^{5}_{\Lambda}$He and $^{12}_{\Lambda}$C. Due to the reduction of interferences, two-nucleon coincidences are expected to give a cleaner determination of Γ_n/Γ_p than single-nucleon observables. Single-nucleon distributions are found to be less sensitive to variations of Γ_n/Γ_p than double-coincidence spectra. The comparison of our results with preliminary KEK coincidence data allows us to extract a Γ_n/Γ_p ratio for $^{5}_{\Lambda}$He of 0.39 ± 0.11 when multinucleon induced channels are omitted.

DOI: 10.1103/PhysRevC.69.054603 PACS number(s): 21.80.+a, 13.30.Eg, 13.75.Ev

I. INTRODUCTION

An old challenge of hypernuclear decay studies has been to secure the "elusive" theoretical explanation of the large experimental values of the ratio between the neutron- and proton-induced nonmesonic decay rates, $\Gamma_n/\Gamma_p \equiv \Gamma(\Lambda n \to nn)/\Gamma(\Lambda p \to np)$ [1,2]. Indeed, the calculations underestimate the data for all considered hypernuclei. Moreover, in the experiments performed until now it has not been possible to distinguish between nucleons produced by the one-body induced channel $\Lambda N \to nN$ and the two-body induced mechanism $\Lambda NN \to nNN$ which is expected to be non-negligible and thus important for the determination of Γ_n/Γ_p.

Because of its strong tensor component, the one-pion-exchange (OPE) model with the $\Delta I = 1/2$ isospin rule supplies very small ratios, typically in the interval 0.05–0.20. On the contrary, the OPE description can reproduce the total nonmesonic decay rates observed for light and medium hypernuclei.

Other interaction mechanisms might then be necessary to correct for the overestimation of Γ_p and the underestimation of Γ_n characteristic of the OPE. Those which have been studied extensively in the literature are the following ones.

(1) The inclusion in the $\Lambda N \to nN$ transition potential of mesons heavier than the pion (also including the exchange of correlated or uncorrelated two pions) [3–7].

(2) The inclusion of interaction terms that explicitly violate the $\Delta I = 1/2$ rule [1,8,9].

(3) The inclusion of the two-body induced decay mechanism [10–13].

(4) The description of the short range $\Lambda N \to nN$ transition in terms of quark degrees of freedom [14,15], which automatically introduces $\Delta I = 3/2$ contributions.

Recent progress has been made on the subject in the following.

(1) On the one hand, a few calculations [5–7,14] with $\Lambda N \to nN$ transition potentials including heavy-meson exchange and/or direct quark contributions obtained ratios more in agreement with data, without providing, nevertheless, an explanation of the origin of the puzzle [1]. In particular, these calculations found a reduction of the proton-induced decay width due to the opposite sign of the tensor component of K exchange with respect to the one for π exchange. Moreover, the parity violating $\Lambda N(^3S_1) \to nN(^3P_1)$ transition, which contributes to both the n- and p-induced processes, is considerably enhanced by K exchange and direct quark mechanisms and tends to increase Γ_n/Γ_p [6,14]. Very recently, the $\Lambda N \to nN$ interaction has been studied within an effective field theory framework [16]. The decay of s- and p-shell hypernuclei was approached following the same formalism as in Refs. [4,6], but the weak transition was described in terms of OPE, one-kaon-exchange, and $|\Delta S| = 1$ four-fermion contact terms. The results obtained in Ref. [16] are very encouraging and open a new door for systematic studies of hypernuclear weak decay based on effective field theory descriptions.

(2) On the other hand, an error in the computer program employed in Ref. [17] to evaluate the single-nucleon energy spectra from nonmesonic decay has been detected and corrected in Ref. [18]. It consisted in the underestimation, by a factor 10, of the nucleon-nucleon collision probabilities entering the intranuclear cascade calculation. The correction of such an error leads to quite different spectral shapes and made it possible to reproduce old experimental data for $^{12}_{\Lambda}$C [19,20] even with a vanishing value of Γ_n/Γ_p (which is a free parameter in the polarization propagator model of Refs. [17,18]). However, when compared with the recent proton energy spectra measured by KEK-E307 [21], the corrected distributions still provide a quite large value of the ratio: $\Gamma_n/\Gamma_p = 0.87 \pm 0.23$ for $^{12}_{\Lambda}$C [22], which is incompatible with pure theoretical estimations, ranging from 0.1 to 0.5.

In the light of these recent developments and of new experiments at KEK [23], FINUDA [24], and BNL [25], it is important to develop different theoretical approaches and strategies for the determination of Γ_n/Γ_p. In a previous paper [26] we discussed some results of an evaluation of nucleon-nucleon coincidence distribution in the nonmesonic weak decay of $^{5}_{\Lambda}$He and $^{12}_{\Lambda}$C hypernuclei. The calculations were per-

formed by combining a one-meson-exchange model describing one-nucleon induced weak decays in finite nuclei with an intranuclear cascade code taking into account the nucleon final state interactions. The two-nucleon induced channel was also taken into account, treating the nuclear finite size effects by means of a local density approximation scheme.

In the present paper we discuss the nucleon correlation observables in a more systematic way. In order to stress the importance of the coincidence analysis in connection with the determination of Γ_n/Γ_p, we also discuss single-nucleon distributions. In principle, the correlation observables permit a *cleaner* extraction of Γ_n/Γ_p from data than single-nucleon observables. This is due to the elimination of interference terms between *n*- and *p*-induced decays [1], which are unavoidable in experimental data and cannot be taken into account by the Monte Carlo methods usually employed to simulate the nucleon propagation through the residual nucleus. We also perform a weak interaction model independent analysis to extract an estimate for Γ_n/Γ_p using preliminary results from KEK [23,27] on two-nucleon angular and energy correlations. The resulting Γ_n/Γ_p values for ${}^{5}_{\Lambda}$He turn out to be substantially smaller than those obtained in the past [20,28] from single coincidence analyses and fall within the predictions of recent theoretical studies [6,7,14].

The work is organized as follows. In Sec. II we give an outline of the models employed to describe the nonmesonic weak decay. In Sec. III we discuss the main features of the Monte Carlo simulation accounting for the nucleon propagation inside the residual nucleus. The purpose of Sec. IV is to discuss the reasons why multinucleon coincidence analyses should be preferred over single-nucleon studies in order to extract Γ_n/Γ_p from data. Our results are discussed in Sec. V and the conclusions are given in Sec. VI.

II. MODELS FOR THE WEAK DECAY

A. One-nucleon induced decay: finite nucleus approach

The one-nucleon induced nonmesonic decay rate can be written as

$$\Gamma_1 = \int \frac{d^3P_T}{(2\pi)^3} \int \frac{d^3k_r}{(2\pi)^3} (2\pi)\,\delta(M_H - E_R - E_1 - E_2) \times \frac{1}{(2J+1)} \sum_{\substack{M_J\{R\} \\ \{1\}\{2\}}} |\mathcal{M}_{fi}|^2,$$

where the initial hypernucleus, of mass M_H, is assumed to be at rest and the quantities E_R and $E_{1,2}$ are the total energy of the residual nuclear system and the total asymptotic energies of the emitted nucleons, respectively. The integration variables $\vec{P}_T \equiv \vec{k}_1 + \vec{k}_2$ and $\vec{k}_r \equiv (\vec{k}_1 - \vec{k}_2)/2$ are the total and relative momenta of the two outgoing nucleons. The momentum conserving δ function has been used to integrate out the momentum of the residual nucleus, $\vec{k}_R = -\vec{P}_T$. The sum, together with the factor $1/(2J+1)$, indicates an average over the initial hypernucleus total spin projections M_J and a sum over all quantum numbers of the residual system $\{R\}$ as well as over the spin and isospin projections of the outgoing nucleons, $\{1\}$ and $\{2\}$. Finally

$$\mathcal{M}_{fi} = \langle \Psi_R; \vec{P}_T\, \vec{k}_r, S\, M_S, T\, T_3 | \hat{O}_{\Lambda N \to nN} | \Psi_H \rangle$$

is the amplitude for the transition from an initial hypernuclear state Ψ_H into a final state which is factorized into an antisymmetrized two-nucleon state and a residual nuclear state Ψ_R. The two-nucleon state is characterized by the total momentum $\vec{P}_T$, the relative momentum $\vec{k}_r$, the spin and spin projection S, M_S, and the isospin and isospin projection T, T_3. Finally, $\hat{O}_{\Lambda N \to nN}$ is a two-body transition operator acting on all possible ΛN pairs.

Working in a coupled two-body spin and isospin basis, the nonmesonic decay rate can be written as

$$\Gamma_1 = \Gamma_n + \Gamma_p,$$

where Γ_n and Γ_p stand for the neutron- $(\Lambda n \to nn)$ and proton-induced $(\Lambda p \to np)$ decay rate, respectively. They are given by $(N = n, p)$

$$\begin{aligned}
\Gamma_N = \int \frac{d^3P_T}{(2\pi)^3} \int \frac{d^3k_r}{(2\pi)^3} (2\pi)\,\delta(M_H - E_R - E_1 - E_2) \sum_{SM_S} \sum_{J_R M_R} \sum_{T_R T_{3_R}} \frac{1}{2J+1} \sum_{M_J} \left| \left\langle T_R T_{3_R},\ \frac{1}{2} t_{3N} \middle| T_I T_{3_I} \right\rangle \right|^2 \\
\times \left| \sum_{TT_3} \left\langle TT_3 \middle| \frac{1}{2} - \frac{1}{2}, \frac{1}{2} t_{3N} \right\rangle \sum_{m_\Lambda M_C} \langle j_\Lambda m_\Lambda, J_C M_C | J M_J \rangle \sum_{j_N} S^{1/2}(J_C T_I; J_R T_R, j_N t_{3N}) \sum_{M_R m_N} \langle J_R M_R, j_N m_N | J_C M_C \rangle \right. \\
\times \sum_{m_{l_N} m_{s_N}} \left\langle j_N m_N \middle| l_N m_{l_N}, \frac{1}{2} m_{s_N} \right\rangle \sum_{m_{l_\Lambda} m_{s_\Lambda}} \left\langle j_\Lambda m_\Lambda \middle| l_\Lambda m_{l_\Lambda}, \frac{1}{2} m_{s_\Lambda} \right\rangle \sum_{S_0 M_{S_0}} \left\langle S_0 M_{S_0} \middle| \frac{1}{2} m_{s_\Lambda}, \frac{1}{2} m_{s_N} \right\rangle \\
\left. \times \sum_{T_0 T_{3_0}} \left\langle T_0 T_{3_0} \middle| \frac{1}{2} - \frac{1}{2}, \frac{1}{2} t_{3N} \right\rangle \frac{1 - (-1)^{(L+S+T)}}{\sqrt{2}} t_{\Lambda N \to nN}(S, M_S, T, T_3, S_0, M_{S_0}, T_0, T_{3_0}, l_\Lambda, l_N, \vec{P}_T, \vec{k}_r) \right|^2, \qquad (1)
\end{aligned}$$

where $S^{1/2}(J_C\ T_I; J_R\ T_R, j_N\ t_{3N})$ is a nucleon pickup spectroscopic amplitude, $t_{3p}=1/2$ and $t_{3n}=-1/2$. The elementary amplitude $t_{\Lambda N\to nN}$ accounts for the transition from an initial ΛN state with spin (isospin) S_0 (T_0) to a final antisymmetric nN state with spin (isospin) $S(T)$. It can be written in terms of other elementary amplitudes which depend on center of mass ("R") and relative ("r") orbital angular momentum quantum numbers of the ΛN and nN systems:

$$t_{\Lambda N\to nN}=\sum_{N_rL_rN_RL_R} X(N_rL_r,N_RL_R,l_\Lambda l_N)t^{N_rL_r\ N_RL_R}_{\Lambda N\to nN}, \qquad (2)$$

where the dependence on the spin and isospin quantum numbers has to be understood. In Eq. (2), the coefficients $X(N_rL_r,N_RL_R,l_\Lambda l_N)$ are the well known Moshinsky brackets, while

$$t^{N_rL_rN_RL_R}_{\Lambda N\to nN}=\frac{1}{\sqrt{2}}\int d^3R\int d^3r\ \mathrm{e}^{-i\vec{P}_T\cdot\vec{R}}\Psi^*_{\vec{k}_r}(\vec{r})\chi^{\dagger S}_{M_S}\chi^{\dagger T}_{T_3}$$
$$\times V_{\sigma,\tau}(\vec{r})\Phi^{\mathrm{c.m.}}_{N_RL_R}\left(\frac{\vec{R}}{b/\sqrt{2}}\right)\Phi^{\mathrm{rel}}_{N_rL_r}\left(\frac{\vec{r}}{\sqrt{2}b}\right)\chi^{S_0}_{M_{S_0}}\chi^{T_0}_{T_{3_0}}. \qquad (3)$$

Here, $V_{\sigma,\tau}(\vec{r})$ stands for the one-meson-exchange weak potential, which depends on the relative distance between the interacting Λ and nucleon as well as on their spin and isospin quantum numbers. Moreover, $\Phi^{\mathrm{rel}}_{N_rL_r}[\vec{r}/(\sqrt{2}b)]$ and $\Phi^{\mathrm{c.m.}}_{N_RL_R}[\vec{R}/(b/\sqrt{2})]$ are the relative and center-of-mass harmonic oscillator wave functions describing the ΛN system, while $\Psi^-_{k_r}(\vec{r})$ is the relative wave function of the nN final state. Further details regarding notation can be found in Ref. [4].

In order to study nucleon-nucleon coincidence spectra, it is convenient to introduce differential decay widths depending on the center-of-mass coordinate $\vec{R}$, the cosinus of the angle between nucleon 1 and 2, cos θ_{12}, and the modulus of the momentum of one of the outgoing nucleons, say k_1. For this purpose, taking into account Eqs. (2) and (3), let us rewrite the decay rate of Eq. (1) in the following schematic way:

$$\Gamma_N=\int d^3P_T\int d^3k_r\sum_i a_i\left[\sum_j c_j\int d^3R A_{ij}(\vec{R},\vec{P}_T,\vec{k}_r)\right]$$
$$\times\left[\sum_{j'}c^*_{j'}\int d^3R' A^*_{ij'}(\vec{R}',\vec{P}_T,\vec{k}_r)\right]$$
$$\equiv\int d^3P_T\int d^3k_r\int d^3R\Gamma_N(\vec{R},\vec{P}_T,\vec{k}_r), \qquad (4)$$

where a_i and c_j include Clebsh-Gordan coefficients and other factors that depend on various quantum numbers, while $A_{ij}(\vec{R},\vec{P}_T,\vec{k}_r)$ denote $\Lambda N\to nN$ weak decay amplitudes. Changing variables from $\vec{P}_T,\vec{k}_r$ to $\vec{k}_1,\vec{k}_2$, using the energy conserving δ function and imposing rotational invariance, it is possible to substitute, in the integrand of Eq. (4), the $\vec{k}_r$ and $\vec{P}_T$ dependence by a dependence on k_1 and cos θ_{12}.

TABLE I. Weak decay rates (in units of the free Λ decay width) predicted by Ref. [6] for $^5_\Lambda$He and $^{12}_\Lambda$C.

	$\Gamma_n+\Gamma_p$			Γ_n/Γ_p		
	OPE	OMEa	OMEf	OPE	OMEa	OMEf
$^5_\Lambda$He	0.43	0.43	0.32	0.09	0.34	0.46
$^{12}_\Lambda$C	0.75	0.73	0.55	0.08	0.29	0.34

Without performing the $\vec{R}$, k_1, and cos θ_{12} integrations, one can then write n- and p-stimulated differential decay rates

$$\Gamma_N(\vec{R},k_1,\cos\ \theta_{12})=\sum_i a_i\left[\sum_j c_jA_{ij}(\vec{R},k_1,\cos\ \theta_{12})\right]$$
$$\times\left[\sum_{j'}c^*_{j'}\int d^3R' A^*_{ij'}(\vec{R}',k_1,\cos\ \theta_{12})\right], \qquad (5)$$

appropriate for obtaining the distributions of the weak decay nucleons required as input of the intranuclear cascade calculation. As explained in the following section, the intranuclear cascade code allows then the primary nucleons to change energy, direction, and charge, exciting other secondary nucleons that are also followed as they move through the nucleus.

Note that by considering the primary nucleons as emerging from the same point $\vec{R}$ in space, we have implicitly assumed that the weak transition proceeds as a point interaction. This is implied by the shape of the regularized potentials of the model of Refs. [4,6]—shown in Ref. [29]—which peak at relative distances $r\equiv|\vec{r}_1-\vec{r}_2|\lesssim 0.5$ fm.

Finally, we recall that in our calculations the one-meson-exchange (OME) weak transition potential entering Eq. (3) contains the exchange of ρ, K, K^*, ω, and η mesons in addition to the pion [6]. The strong couplings and strong final state interactions acting between the weak decay nucleons are taken into account by using a scattering nN wave function from the Lippmann-Schwinger (T-matrix) equation obtained with NSC97 (versions "a" and "f") potentials [30]. The corresponding decay rates for $^5_\Lambda$He and $^{12}_\Lambda$C are listed in Table I (OMEa and OMEf) together with the OPE predictions.

B. Two-nucleon induced decay: local density approximation

The differential and total decay rates for the two-nucleon induced process $\Lambda np\to nnp$ are calculated with the polarization propagator method in local density approximation (LDA) of Refs. [11,12]. In such a calculation, the simple OPE mechanism, supplemented by strong ΛN and nN short range correlations (given in terms of phenomenological Landau functions) described the weak transition process. The two-nucleon induced differential decay width $\Gamma_2(\vec{R},k_1,\cos\ \theta_{12})$ is obtained from the two-particle two-hole ($2p2h$) contributions to the pion self-energy. As explained in Ref. [11], these contributions are derived in a phenomenological way from a fit to pionic atoms, conveniently modified

by the Lorentz-Lorenz correction and extended to all kinematical regions using the appropriate phasespace. The intranuclear cascade code then follows the fate of the two nucleons excited by these $2p2h$ components, as well as that of the third nucleon emitted at the $\Lambda N\pi$ vertex, as they move through the nucleus.

In the present calculation, the distributions of the weak decay nucleons and the value of Γ_2 have been properly scaled to maintain the ratio Γ_2/Γ_1 unchanged: we then use $\Gamma_2/\Gamma_1 \equiv (\Gamma_2/\Gamma_1)^{\mathrm{LDA}} = 0.20$ for ${}^{5}_{\Lambda}$He and 0.25 for ${}^{12}_{\Lambda}$C. These values of $(\Gamma_2/\Gamma_1)^{\mathrm{LDA}}$ have been obtained with the latest update of parameters given in Ref. [12] after correcting a small (conceptual) error in the implementation of data on the *P*-wave pion-nucleus optical potential. For the hypernuclei treated in the present paper, ${}^{5}_{\Lambda}$He and ${}^{12}_{\Lambda}$C, such a correction slightly decreases the values of Γ_1 while increasing Γ_2 by about 20%.

III. INTRANUCLEAR CASCADE SIMULATION

In their way out of the nucleus, the weak decay (i.e., primary) nucleons continuously change energy, direction, and charge due to collisions with other nucleons. As a consequence, secondary nucleons are also emitted.

We simulate the nucleon propagation inside the residual nucleus with the Monte Carlo code of Refs. [17,18]. A random number generator determines the decay channel, *n*-, *p*-, or two-nucleon induced, according to the ratios Γ_n/Γ_p and Γ_2/Γ_1 predicted by our finite nucleus and LDA approaches. Positions, momenta, and charges of the weak decay nucleons are selected by the same random number generator, according to the corresponding probability distributions given by the finite nucleus and LDA calculations.

For neutron-, proton- and two-nucleon induced decays, the discussion of Sec. II allows us to introduce the differential decay rates $\Gamma_n(\vec{R},k_1,\cos\theta_{12})$, $\Gamma_p(\vec{R},k_1,\cos\theta_{12})$, and $\Gamma_2(\vec{R},k_1,\cos\theta_{12})$ supplying the *n*-, *p*- and two-nucleon stimulated total rates Γ_n, Γ_p, and Γ_2 through the following relation:

$$\Gamma_i = \int d^3k_1 \int d\cos\theta_{12} \int d^3R\, \Gamma_i(\vec{R},k_1,\cos\theta_{12}).$$

After they are produced as explained, the primary nucleons move under a local potential $V_N(R) = -k^2_{F_N}(R)/2m_N$, where $k_{F_N}(R) = [3\pi^2\rho_N(R)]^{1/3} (N = n,p)$ is the local nucleon Fermi momentum corresponding to the nucleon density $\rho_N(R)$. The primary nucleons also collide with other nucleons of the medium according to free space nucleon-nucleon cross sections [31] properly corrected to take into account the Pauli blocking effect. For further details concerning the intranuclear cascade calculation see Ref. [17]. Each Monte Carlo event will then end with a certain number of nucleons which leave the nucleus along defined directions and with defined energies. One can then select the outgoing nucleons and store them in different ways, as we shall do in the discussion of Sec. V.

We are aware of the fact that accounting for nucleon final state interactions effects in light residual nuclei (as those required to treat ${}^{5}_{\Lambda}$He) through Monte Carlo techniques is questionable. However, realistic calculations for few-body scattering states have been performed up to three nucleons only (see for instance Ref. [32]). For the hypernuclear nonmesonic decay problem, only the case of ${}^{3}_{\Lambda}$H has been treated exactly [29,33]. Although one might attempt three-cluster-type calculations, this goes beyond the scope of the present work. For this reason, the results we present for ${}^{5}_{\Lambda}$He should be considered less realistic than the corresponding ones for ${}^{12}_{\Lambda}$C.

IV. SINGLE-NUCLEON VERSUS NUCLEON-COINCIDENCE ANALYSES

In this section we discuss the reason why multinucleon coincidence studies should be preferred over single-nucleon analyses when the purpose is the determination of Γ_n/Γ_p. The argument—of both theoretical and experimental origin—for this explanation is based on the reduction of quantum mechanical *interferences* between *n*- and *p*-stimulated weak decays [1].

Let us first note that the nucleons originating from *n*- and *p*-induced processes are added *incoherently* (i.e., classically) in our intranuclear cascade calculation (for the moment we are then neglecting an analogous effect due to the two-nucleon stimulated decay channel). However, for particular kinematics of the detected nucleons (for instance, at low-kinetic energies), a possible quantum-mechanical interference effect between *n*- and *p*-induced channels should inevitably affect the observed distributions. Therefore, extracting the ratio Γ_n/Γ_p from experimental data with the help of a classical intranuclear cascade calculation may not be a clean task.

To clarify better the issue, let us consider for instance an experiment (such as the majority of the experiments performed up to now) measuring *single-proton* kinetic energy spectra. The relevant quantity is then the number of outgoing protons observed as a function of the kinetic energy T_p. Schematically, this observable can be written as

$$N_p(T_p) \propto |\langle p(T_p)|\hat{O}_{\mathrm{FSI}}\,\hat{O}_{\mathrm{WD}}|\Psi_H\rangle|^2 = |\alpha\langle p(T_p)|\hat{O}_{\mathrm{FSI}}|nn,\Psi_R\rangle + \beta\langle p(T_p)|\hat{O}_{\mathrm{FSI}}|np,\Psi_{R'}\rangle|^2, \quad (6)$$

where $|p(T_p)\rangle$ represents a many-nucleon final state with a proton whose kinetic energy is T_p. Moreover, in Eq. (6) the action of the weak decay operator $\hat{O}_{\mathrm{WD}} \equiv \hat{O}_{\Lambda n\to nn} + \hat{O}_{\Lambda p\to np}$ produced the superposition

$$\hat{O}_{\mathrm{WD}}|\Psi_H\rangle = \alpha|nn,\Psi_R\rangle + \beta|np,\Psi_{R'}\rangle.$$

Here $|nn,\Psi_R\rangle (|np,\Psi_{R'}\rangle)$ is a state with a $nn(np)$ primary pair moving inside a residual nucleus $\Psi_R(\Psi_{R'})$. Note that in the present schematic picture: $\Gamma_n \propto |\alpha|^2$ and $\Gamma_p \propto |\beta|^2$. Since both transition amplitudes entering the last equality of Eq. (6) are in general nonvanishing, interference terms between *n*- and *p*-induced decays are expected to contribute to $N_p(T_p)$. An amplitude $\langle p(T_p)|\hat{O}_{\mathrm{FSI}}|nn,\Psi_R\rangle$ different from zero means that, due to nucleon final state interactions

(FSI), a secondary proton has a nonvanishing probability to emerge from the nucleus with kinetic energy T_p even if the weak process was *n* induced (i.e., without primary protons). While for high kinetic energies (say for $T_p > 80$ MeV) this amplitude is expected to be almost vanishing, as long as T_p decreases its contribution could produce an important interference effect (see the results discussed in Sec. V A).

An interference-free observation would imply the measurement of all the quantum numbers of the final nucleons and residual nucleus. While this is an impossible experiment, what is certain is that the magnitude of the interference can be reduced if one measures in a more accurate way the final state. For this reason, two-nucleon coincidence observables are expected to be less affected by interferences than single-nucleon ones and thus more reliable for determining Γ_n/Γ_p. If we consider the detection of the kinetic energy *correlation* of *np* pairs emitted nearly back to back (say with $\cos\theta_{np} \leqslant -0.9$)

$$N_{np}(T_n + T_p, \cos\theta_{np} \leqslant -0.9) \propto |\alpha\langle n(T_n), p(T_p), \cos\theta_{np} \leqslant -0.9|\hat{O}_{\mathrm{FSI}}|nn, \Psi_R\rangle + \beta\langle n(T_n), p(T_p), \cos\theta_{np} \leqslant -0.9|\hat{O}_{\mathrm{FSI}}|np, \Psi_{R'}\rangle|^2, \tag{7}$$

one expects an interference effect smaller than the one appearing in single-nucleon observations, i.e., in Eq. (6), especially when particular energy cuts are considered.

To see this more explicitly, let us rewrite Eqs. (6) and (7) in the following way:

$$N_p = [N_p^{\Lambda n\to nn} + N_p^{\Lambda p\to np}][1 + I_p \cos\phi_p], \tag{8}$$

$$N_{np} = [N_{np}^{\Lambda n\to nn} + N_{np}^{\Lambda p\to np}][1 + I_{np} \cos\phi_{np}], \tag{9}$$

where the various arguments have been suppressed and the number of nucleons

$$N_p^{\Lambda n\to nn} \equiv |A_p^{\Lambda n\to nn}|^2 \propto |\alpha|^2|\langle p|\hat{O}_{\mathrm{FSI}}|nn, \Psi_R\rangle|^2,$$

$$N_p^{\Lambda p\to np} \equiv |A_p^{\Lambda p\to np}|^2 \propto |\beta|^2|\langle p|\hat{O}_{\mathrm{FSI}}|np, \Psi_{R'}\rangle|^2,$$

$$N_{np}^{\Lambda n\to nn} \equiv |A_{np}^{\Lambda n\to nn}|^2 \propto |\alpha|^2|\langle np|\hat{O}_{\mathrm{FSI}}|nn, \Psi_R\rangle|^2,$$

$$N_{np}^{\Lambda p\to np} \equiv |A_{np}^{\Lambda p\to np}|^2 \propto |\beta|^2|\langle np|\hat{O}_{\mathrm{FSI}}|np, \Psi_{R'}\rangle|^2,$$

have obvious meaning. Moreover

$$I_p = \frac{2\sqrt{N_p^{\Lambda n\to nn}\, N_p^{\Lambda p\to np}}}{N_p^{\Lambda n\to nn} + N_p^{\Lambda p\to np}},$$

$$I_{np} = \frac{2\sqrt{N_{np}^{\Lambda n\to nn}\, N_{np}^{\Lambda p\to np}}}{N_{np}^{\Lambda n\to nn} + N_{np}^{\Lambda p\to np}},$$

and $\phi_p = \phi_p^{\Lambda n\to nn} - \phi_p^{\Lambda p\to np}$ ($\phi_{np} = \phi_{np}^{\Lambda n\to nn} - \phi_{np}^{\Lambda p\to np}$) is the phase difference between the amplitudes $A_p^{\Lambda n\to nn} = \sqrt{N_p^{\Lambda n\to nn}}\, e^{i\phi_p^{\Lambda n\to nn}}$ and $A_p^{\Lambda p\to np} = \sqrt{N_p^{\Lambda p\to np}}\, e^{i\phi_p^{\Lambda p\to np}}$ ($A_{np}^{\Lambda n\to nn} = \sqrt{N_{np}^{\Lambda n\to nn}}\, e^{i\phi_{np}^{\Lambda n\to nn}}$ and $A_{np}^{\Lambda p\to np} = \sqrt{N_{np}^{\Lambda p\to np}}\, e^{i\phi_{np}^{\Lambda p\to np}}$). Note that the distributions of Eq. (8) [Eq. (9)] are not affected by interference only when $I_p \cos\phi_p = 0$ [$I_{np} \cos\phi_{np} = 0$]. Since, as explained, we expect $N_{np}^{\Lambda n\to nn}/N_{np}^{\Lambda p\to np} < N_p^{\Lambda n\to nn}/N_p^{\Lambda p\to np} < 1$, then I_{np} will be smaller than I_p. The numerical results discussed in Sec. V A and V B confirm this expectation.

The same reasoning must be applied—and the previous equations changed accordingly—once the two-nucleon induced decay mechanism is taken into account.

Note, however, that our discussion in this section has disregarded the effect of the phase differences ϕ_p and ϕ_{np}, which cannot be evaluated theoretically. An indirect estimate of these phases (and then of the real interference effects) can be obtained through the comparison of our calculated spectra (in which interference is not taken into account) with the experimental ones (which could be affected by interferences). In Sec. V B we discuss an indirect indication for a small interference effect in double-coincidence observables.

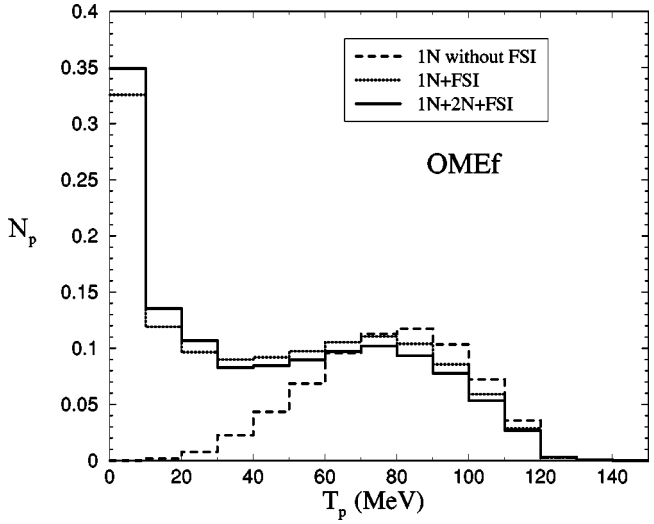

FIG. 1. Single-*proton* kinetic energy spectra for the nonmesonic decay of ${}^{5}_{\Lambda}$He. The dashed and dotted lines are normalized *per one-nucleon induced decay* ($\Gamma_1 = \Gamma_n + \Gamma_p$), while the continuous line is normalized *per nonmesonic decay* ($\Gamma_{\mathrm{NM}} = \Gamma_1 + \Gamma_2$).

V. RESULTS

A. Single-nucleon spectra

In Figs. 1 and 2 we show the proton kinetic energy spectra corresponding to the decay of ${}^{5}_{\Lambda}$He and ${}^{12}_{\Lambda}$C, respectively. Note the particular normalizations of the curves presented in this and in the following figures. The dashed curves correspond to the distributions of the one-nucleon induced primary protons: they have been obtained through intranuclear cascade calculations in which the one-nucleon stimulated weak decay nucleons move under the effect of the nuclear local potential, $V_N(R) = -k_{F_N}^2(R)/2m_N$, without colliding with the nucleons of the medium. The inclusion of nucleon FSI provide the result given by the dotted lines. The continuous

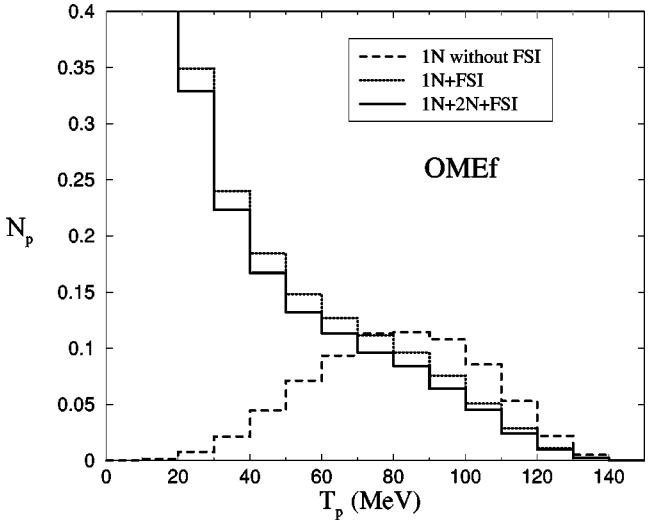

FIG. 2. Same as in Fig. 1 for $^{12}_{\Lambda}$C.

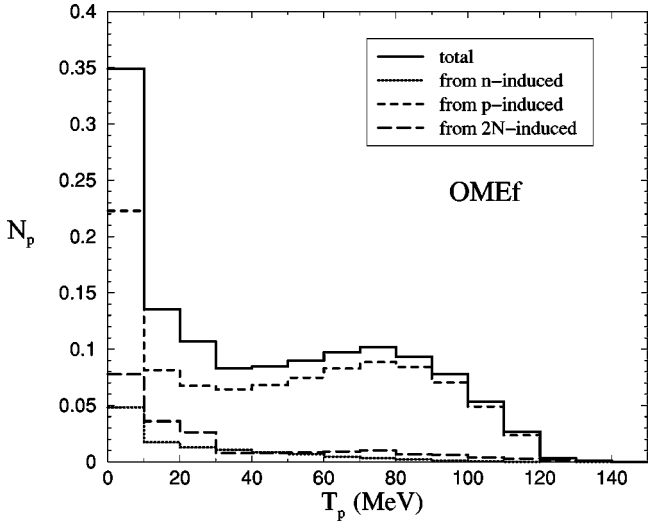

FIG. 3. Single-*proton* kinetic energy spectra for the nonmesonic weak decay of $^{5}_{\Lambda}$He. The total spectrum N_p (normalized *per nonmesonic weak decay*) has been decomposed in its components $N_p^{\Lambda n\to nn}$, $N_p^{\Lambda p\to np}$, and $N_p^{\Lambda np\to nnp}$ according to Eq. (10).

lines correspond to the full calculation, i.e., once the two-nucleon induced channel is also included. The calculations have been performed with the OMEf model, which predicts $\Gamma_n/\Gamma_p=0.46$ for $^{5}_{\Lambda}$He and $\Gamma_n/\Gamma_p=0.34$ for $^{12}_{\Lambda}$C. The model OMEa supplies similar results both for the proton and neutron spectra. While the primary proton distributions are very similar for the two hypernuclei (the one for $^{12}_{\Lambda}$C is slightly broader), the full calculations clearly show that, as expected, FSI have a bigger effect for the heavier system. For $^{12}_{\Lambda}$C, FSI are so important that they completely smear out the maxima corresponding to the primary protons. Our predictions for the proton spectra from $^{12}_{\Lambda}$C should be compared with the one measured at KEK-E307 [21]. Unfortunately, this is not possible since these data have not been corrected for the detector geometry and the energy losses occurring in the target and detector materials.

Let us now introduce the number of nucleons of the type $N(N=n,p)$ produced in n-induced ($N_N^{1\mathrm{Bn}}$), p-induced ($N_N^{1\mathrm{Bp}}$), and two-nucleon induced ($N_N^{2\mathrm{B}}$) decays. If we normalize these quantities per n-induced, p-induced, and two-nucleon induced decay, respectively, the *total* number of nucleons of the type N (normalized per nonmesonic weak decay) is given by

$$N_N=\frac{N_N^{1\mathrm{Bn}}\Gamma_n+N_N^{1\mathrm{Bp}}\Gamma_p+N_N^{2\mathrm{B}}\Gamma_2}{\Gamma_n+\Gamma_p+\Gamma_2}\equiv N_N^{\Lambda n\to nn}+N_N^{\Lambda p\to np}+N_N^{\Lambda np\to nnp},\qquad(10)$$

where $N_N^{\Lambda n\to nn}$, $N_N^{\Lambda p\to np}$ and $N_N^{\Lambda np\to nnp}$ have obvious meaning. All these nucleon numbers can be considered either as being functions of the nucleon kinetic energy, $N_N(T_N)$, as it is the case of Figs. 1 and 2, or as the corresponding integrated quantities, $N_N=\int dT_N N_N(T_N)$. By construction, $N_N^{1\mathrm{Bn}}$, $N_N^{1\mathrm{Bp}}$, and $N_N^{2\mathrm{B}}$ ($N_N^{\Lambda n\to nn}$, $N_N^{\Lambda p\to np}$ and $N_N^{\Lambda np\to nnp}$) *do not* depend (*do* depend) on the interaction model employed to describe the weak decay. The number of protons produced per neutron-induced weak decay $N_p^{1\mathrm{Bn}}$ has been evaluated numerically by imposing $\Gamma_p=\Gamma_2=0$ in our calculation code, thereby selecting the $\Lambda n\to nn$ mode as the only allowed decay process. The two primary neutrons will then collide with other nucleons of the medium producing a final amount of outgoing protons $N_p^{1\mathrm{Bn}}$ per neutron-induced decay event. Analogous calculations are performed to determine the other nucleon numbers entering Eq. (10).

In Figs. 3 and 4, N_N, $N_N^{\Lambda n\to nn}$, $N_N^{\Lambda p\to np}$, and $N_N^{\Lambda np\to nnp}$ are shown as functions of the nucleon kinetic energy in the case of $^{5}_{\Lambda}$He. In Figs. 5 and 6 the same quantities are given for $^{12}_{\Lambda}$C. From the N_n and N_p distributions for $^{5}_{\Lambda}$He we note that the maxima occurring at $T_N\simeq 75$ MeV—mainly due to the kinematics of the weak decay nucleons (see the dashed line in Fig. 1 for protons)—are more pronounced for neutrons than for protons. Note that for any value of the ratio Γ_n/Γ_p,

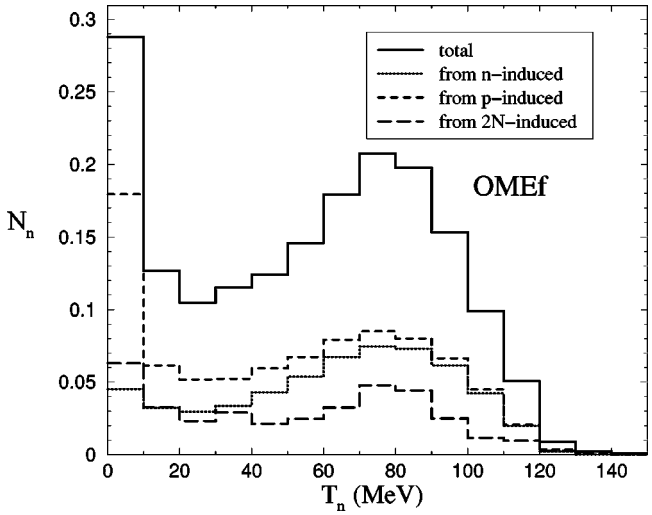

FIG. 4. Single-*neutron* kinetic energy spectra for the nonmesonic weak decay of $^{5}_{\Lambda}$He. The total spectrum N_n (normalized *per nonmesonic weak decay*) has been decomposed in its components $N_n^{\Lambda n\to nn}$, $N_n^{\Lambda p\to np}$, and $N_n^{\Lambda np\to nnp}$ according to Eq. (10).

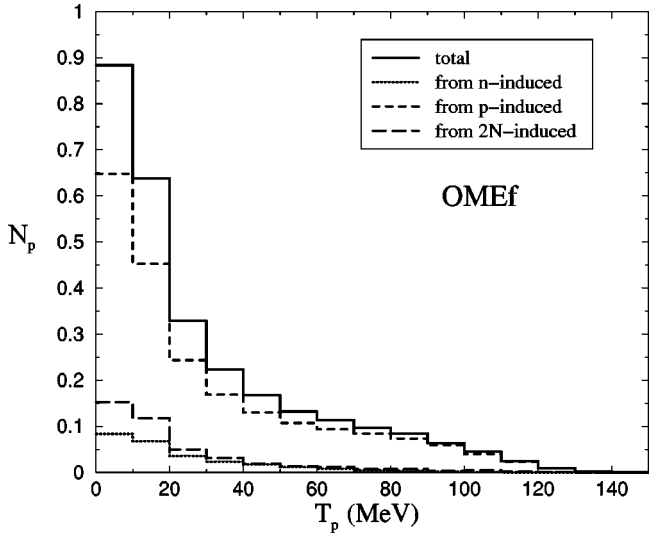

FIG. 5. Same as in Fig. 3 for $^{12}_{\Lambda}$C.

the number of primary neutrons is indeed larger than the number of primary protons [see Eq. (11)]. Consequently, due to neutron-proton reactions, the proportion of secondary protons in the proton spectrum is larger than the proportion of secondary neutrons in the neutron spectrum. From Figs. 3 and 5 we also note that the fractions of *protons* emitted in *neutron*-induced processes are quite small. For values of T_p in the 30–40 MeV bin (i.e., just above the experimental threshold), $N_p^{\Lambda n\to nn}/N_p^{\Lambda p\to np}\simeq 0.15$ both for $^{5}_{\Lambda}$He and $^{12}_{\Lambda}$C, which corresponds to an interference term $I_p \cos\phi_p = 0.67 \cos\phi_p$ in Eq. (8). Therefore, even if the number of protons from *n*-induced decays is expected to be rather small, the existence of such events could nevertheless produce a quite big interference effect: unfortunately, the matter depends crucially on the phase ϕ_p which we cannot estimate theoretically. From Figs. 3 and 5 one also note that the two-nucleon induced mechanism could be responsible for an interference effect in the proton energy spectra as important as the one which could be due to the *n*-induced channel. For

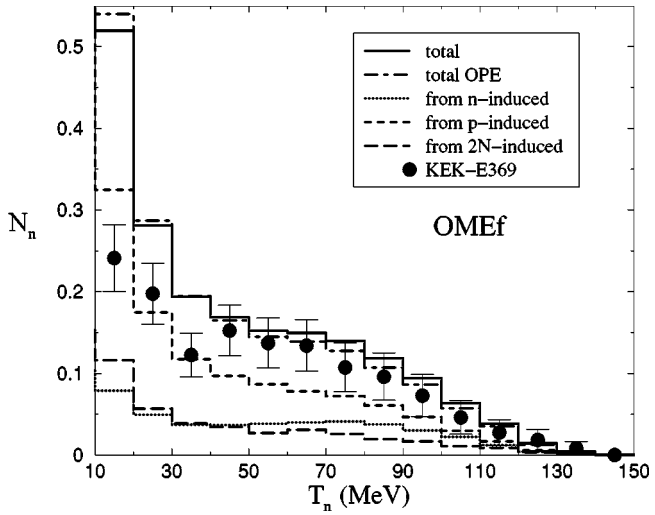

FIG. 6. Same as in Fig. 4 for $^{12}_{\Lambda}$C. The OPE result is also shown. Experimental data are taken from Ref. [34].

single-*neutron* spectra these interference effects could be even larger. Indeed, from Figs. 3–6 it is clear that, as expected, $N_p^{\Lambda n\to nn}/N_p^{\Lambda p\to np} < N_n^{\Lambda n\to nn}/N_n^{\Lambda p\to np} < 1$. Once again this conclusion neglects the effect of the phases of the interfering amplitudes.

The single-neutron spectrum for $^{12}_{\Lambda}$C observed in the KEK-E369 experiment [34] is well reproduced by our calculations. This is evident from Fig. 6, where we show results based on two models (OPE and OMEf) which predict quite different Γ_n/Γ_p ratios. Unfortunately, the dependence of the neutron spectra on variations of Γ_n/Γ_p is very weak (the same is true also for the proton spectra) and a precise extraction of the ratio from the KEK-E369 distribution is not possible. We checked that an analogous calculation performed with the polarization propagator method in local density approximation of Ref. [18] supplies neutron spectra which reproduce the data of Fig. 6 with a χ^2 per degrees of freedom smaller than 1 when Γ_n/Γ_p (a free parameter in such kind of calculations) is chosen to lie in the range 0–1.5 and data above $T_n = 30$ MeV are considered. The little sensitivity of N_n and N_p to Γ_n/Γ_p is mainly due to the fact that these numbers are normalized to the same total non-mesonic decay rate (i.e., per nonmesonic weak decay). The non-normalized nucleon spectra, $S_n \equiv N_n\,\Gamma_{\rm NM}$ and $S_p \equiv N_p\,\Gamma_{\rm NM}$ [see Eq. (10)], have indeed a stronger dependence on Γ_n/Γ_p. As a consequence, in order to discriminate between different weak decay models, one should separately compare the complementary observable, $\Gamma_n+\Gamma_p$, with experiment. For $^{12}_{\Lambda}$C, our calculations supply $\Gamma_{\rm NM} \equiv \Gamma_n+\Gamma_p+\Gamma_2 = 1.25(\Gamma_n+\Gamma_p) = 0.91$ or 0.69 when model OMEa or OMEf is used. These values agree quite well with the KEK datum 0.83 ± 0.11 of Ref. [35].

The problem of the small sensitivity of N_n and N_p to variations of Γ_n/Γ_p can be overcome if one concentrates on another single-nucleon observable. The ratio Γ_n/Γ_p is defined in terms of the ratio between the number of primary weak decay neutrons and protons, $N_n^{\rm wd}$ and $N_p^{\rm wd}$, in the following way:

$$\frac{\Gamma_n}{\Gamma_p} \equiv \frac{1}{2}\left(\frac{N_n^{\rm wd}}{N_p^{\rm wd}} - 1\right). \tag{11}$$

Due to two-body induced decays and (especially) nucleon FSI, one expects the inequality

$$\frac{\Gamma_n}{\Gamma_p} \neq \frac{1}{2}\left(\frac{N_n}{N_p} - 1\right) \equiv R_1[\Delta T_n, \Delta T_p, \Gamma_2] \tag{12}$$

to be valid in a situation, such as the experimental one, in which particular intervals of variability of the neutron and proton kinetic energy, ΔT_n and ΔT_p, are employed in the determination of N_n and N_p.

As one can deduce from previous figures, not only N_n and N_p but also the ratio N_n/N_p depends on ΔT_n and ΔT_p. This is more evident from Table II, in which the function R_1 defined by Eq. (12) is given for $^{5}_{\Lambda}$He and $^{12}_{\Lambda}$C, for different nucleon energy thresholds $T_N^{\rm th}$ and for the OPE, OMEa, and OMEf models. For a given energy threshold, R_1 is closer to Γ_n/Γ_p for $^{5}_{\Lambda}$He than for $^{12}_{\Lambda}$C since FSI are larger in carbon. The ratio N_n/N_p (or equivalently R_1) is more sensitive to variations of

TABLE II. Predictions for the quantity R_1 of Eq. (12) for $^{5}_{\Lambda}$He and $^{12}_{\Lambda}$C corresponding to different nucleon thresholds $T_N^{\rm th}$ and to the OPE, OMEa, and OMEf models.

		$T_N^{\rm th}$ (MeV)			
		0	30	60	Γ_n/Γ_p
$^{5}_{\Lambda}$He	OPE	0.04	0.13	0.16	0.09
	OMEa	0.15	0.32	0.39	0.34
	OMEf	0.19	0.40	0.49	0.46
$^{12}_{\Lambda}$C	OPE	−0.06	−0.01	0.05	0.08
	OMEa	−0.02	0.07	0.19	0.29
	OMEf	−0.01	0.09	0.21	0.34

Γ_n/Γ_p (see the differences between the OPE, OMEa, and OMEf calculations of Table II) than N_n and N_p separately. Moreover, N_n/N_p is less affected by FSI than N_n and N_p. Therefore, measurements of N_n/N_p should permit to determine Γ_n/Γ_p with better precision. The recent KEK-E462 experiment has measured the ratio N_n/N_p for $^{5}_{\Lambda}$He: a preliminary analysis of the data supplies a value of R_1 around 0.6 with a relative error of about 20% using nucleon energy thresholds of 50 and 60 MeV [36]. Our result of Table II corresponding to the OMEf calculation for $T_N^{\rm th}=60$ MeV agree with this experimental determination. According to this comparison, the ratio Γ_n/Γ_p for $^{5}_{\Lambda}$He should be around the value 0.46 predicted by the OMEf model.

B. Double-coincidence spectra

In Fig. 7 we report the opening angle distribution of *np* pairs emitted in the nonmesonic decay of $^{5}_{\Lambda}$He. Note the particular normalizations of the curves presented in this and in the following figures. Neglecting nucleon FSI and the two-nucleon induced channel, the angular correlation is strongly peaked at $\theta_{np}=180°$ and only 1 pair out of 100 is emitted with an opening angle smaller than 115° (i.e., with $\cos\theta_{np} \geqslant -0.4$). The effect of FSI is to decrease the weak decay nucleon back-to-back distribution (i.e., for $\cos\theta_{np} \leqslant -0.9$) of about 25% and populate, strongly, the spectrum for $\cos\theta_{np} \geqslant -0.8$. The effect of the two-nucleon induced channel is moderate: practically, it only increases the distribution (by about 20%) in the region with $\cos\theta_{np} > 0.4$. When a nucleon kinetic energy cut of 30 MeV is applied, large part of the distribution is removed. This is due to FSI, which leads to a large amount of pairs ($\simeq$70% of the total) in which at least one nucleon has kinetic energy below 30 MeV.

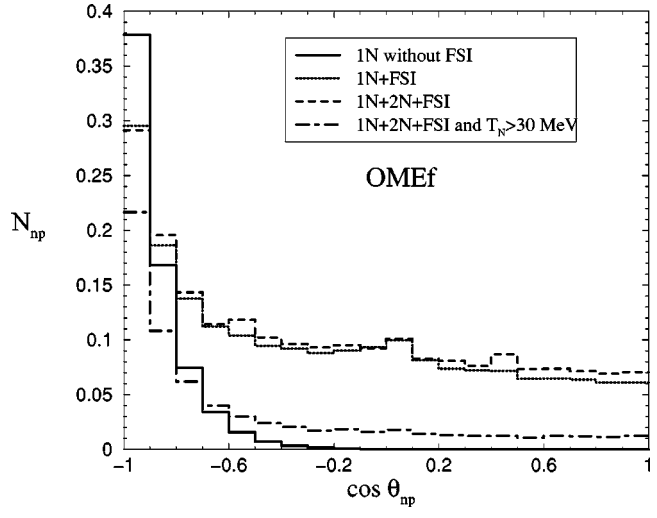

FIG. 7. Opening angle distribution of *np* pairs emitted in the nonmesonic decay of $^{5}_{\Lambda}$He. The continuous and dotted lines are normalized *per one-nucleon induced decay* ($\Gamma_1=\Gamma_n+\Gamma_p$), while the dashed and dot-dashed curves are normalized *per nonmesonic decay* ($\Gamma_{\rm NM}=\Gamma_1+\Gamma_2$).

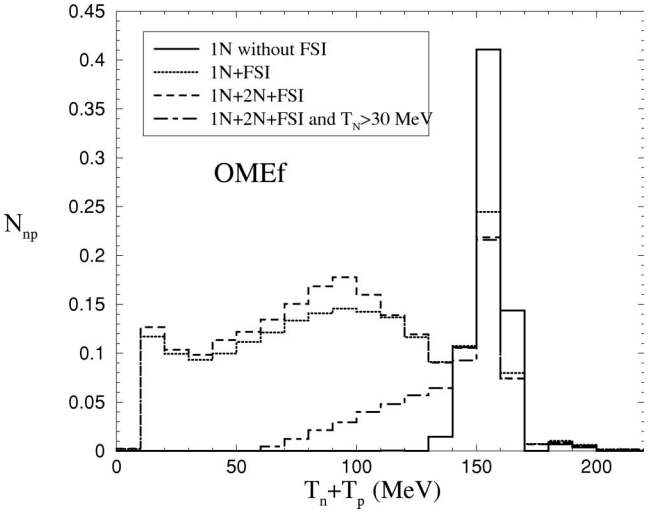

FIG. 8. Kinetic energy sum distribution of *np* pairs emitted in the nonmesonic decay of $^{5}_{\Lambda}$He. The continuous and dotted lines are normalized *per one-nucleon induced decay* ($\Gamma_1=\Gamma_n+\Gamma_p$), while the dashed and dot-dashed curves are normalized *per nonmesonic decay* ($\Gamma_{\rm NM}=\Gamma_1+\Gamma_2$).

In Fig. 8 we show the kinetic energy correlation of *np* pairs emitted in the decay of $^{5}_{\Lambda}$He. Neglecting nucleon FSI and the two-nucleon induced channel, the energy correlation is strongly peaked, as expected, at $T_n+T_p \simeq 155$ MeV. Indeed, the *Q* value corresponding to the proton-induced three-body process $^{5}_{\Lambda}\mathrm{He} \rightarrow {}^{3}\mathrm{H}+n+p$ is 153 MeV. The effect of the FSI is to decrease the back-to-back maximum and to populate, strongly, the spectrum for $T_n+T_p \leqslant 140$ MeV. The effect of the two-nucleon induced channel is only visible when T_n+T_p is below 110 MeV, where it enhances the distribution. Once a 30 MeV kinetic energy cut is applied, the distribution at small T_n+T_p is considerably reduced for the same reason explained in the previous paragraph.

The opening angle and kinetic energy correlations for *nn* pairs have essentially the same structure of the *np* distributions showed in Figs. 7 and 8. For a discussion of the *pp* distributions and the different effect of FSI in $^{5}_{\Lambda}$He and $^{12}_{\Lambda}$C we refer to our previous paper [26].

The ratio Γ_n/Γ_p is defined as the ratio between the number of weak decay *nn* and *np* pairs, $N_{nn}^{\rm wd}$ and $N_{np}^{\rm wd}$. However, due to two-body induced decays and (especially) nucleon FSI effects, one has

TABLE III. OPE, OMEa and OMEf, predictions for N_{np} and its components $N_{np}^{\Lambda n\to nn}$, $N_{np}^{\Lambda p\to np}$, and $N_{np}^{\Lambda np\to nnp}$ (integrated over all angles and for energies $T_N \geqslant 30$ MeV) as given by Eqs. (14) and (15) for the case of $^{12}_{\Lambda}$C. The numbers in parentheses correspond to the angular region with $\cos\theta_{np} \leqslant -0.8$.

	N_{np}	$N_{np}^{\Lambda n\to nn}$	$N_{np}^{\Lambda p\to np}$	$N_{np}^{\Lambda np\to nnp}$
OPE	1.00(0.32)	0.02(0.00)	0.91(0.29)	0.08(0.02)
OMEa	0.89(0.27)	0.06(0.02)	0.76(0.24)	0.08(0.02)
OMEf	0.87(0.27)	0.07(0.02)	0.73(0.23)	0.08(0.02)

$$\frac{\Gamma_n}{\Gamma_p} \equiv \frac{N_{nn}^{\rm wd}}{N_{np}^{\rm wd}} \neq \frac{N_{nn}}{N_{np}} \equiv R_2[\Delta\theta_{12},\Delta T_n,\Delta T_p,\Gamma_2], \qquad (13)$$

when N_{nn} and N_{np} are determined by employing particular intervals of variability of the pair opening angle, $\Delta\theta_{12}$, and the nucleon kinetic energies, ΔT_n and ΔT_p. Actually, as one can deduce from the figures we discussed in Ref. [26], not only N_{nn} and N_{np} but also the ratio N_{nn}/N_{np} depends on $\Delta\theta_{12}$, ΔT_n, and ΔT_p. The discussion of Ref. [26] also proves that the ratio N_{nn}/N_{np} is much less sensitive to FSI effects and variations of the energy cuts and angular restrictions than N_{nn} and N_{np} separately.

The numbers of nucleon pairs N_{NN} discussed up to this point and normalized per nonmesonic weak decay are related to the corresponding quantities for the one-nucleon ($N_{NN}^{\rm 1B}$) and two-nucleon ($N_{NN}^{\rm 2B}$) induced processes [the former (latter) being normalized per one-body (two-body) stimulated nonmesonic weak decay] via the following equation:

$$N_{NN} = \frac{N_{NN}^{\rm 1B}\,\Gamma_1 + N_{NN}^{\rm 2B}\,\Gamma_2}{\Gamma_1+\Gamma_2} \equiv N_{NN}^{\Lambda n\to nn} + N_{NN}^{\Lambda p\to np} + N_{NN}^{\Lambda np\to nnp}, \qquad (14)$$

where

$$N_{NN}^{\rm 1B} = \frac{N_{NN}^{\rm 1Bn}\,\Gamma_n + N_{NN}^{\rm 1Bp}\,\Gamma_p}{\Gamma_1}, \qquad (15)$$

and the remaining N's have obvious meaning. Therefore, the quantities $N_{NN}^{\rm 1Bn}$, $N_{NN}^{\rm 1Bp}$, and $N_{NN}^{\rm 2B}$ ($N_{NN}^{\Lambda n\to nn}$, $N_{NN}^{\Lambda p\to np}$ and $N_{NN}^{\Lambda np\to nnp}$) *do not* depend (*do* depend) on the interaction model employed to describe the weak decay. The number of *np* pairs produced per neutron-induced weak decay $N_{np}^{\rm 1Bn}$ has been evaluated numerically by performing the calculations with $\Gamma_p=\Gamma_2=0$. In this way, the $\Lambda n\to nn$ mode is the only allowed decay process. The intranuclear cascade calculation then starts with two primary neutrons and ends with a number of *np* pairs $N_{np}^{\rm 1Bn}$ which will be emitted by the nucleus per neutron-induced decay event. Analogous calculations are performed to determine the other nucleon numbers entering Eqs. (14) and (15).

In Table III we report the OPE, OMEa, and OMEf predictions for N_{np} and its components $N_{np}^{\Lambda n\to nn}$, $N_{np}^{\Lambda p\to np}$, and $N_{np}^{\Lambda np\to nnp}$ in the case of $^{12}_{\Lambda}$C. Two different opening angle regions and an energy threshold of 30 MeV have been considered. The contribution to N_{np} of the *n*-induced decay channel is always smaller than or comparable with the one coming from the two-nucleon induced mechanism: $N_{np}^{\Lambda n\to nn} \lesssim N_{np}^{\Lambda np\to nnp}$. The ratio $N_{np}^{\Lambda n\to nn}/N_{np}^{\Lambda p\to np}$ is always smaller than 0.10, which corresponds to $I_{np}<0.57$ in Eq. (9). This shows that interferences in coincidence observables are potentially smaller than in single-nucleon spectra but also that they might be non-negligible. Due to the less pronounced effects of FSI in $^{5}_{\Lambda}$He, smaller values of I_{np} have been obtained in this second case.

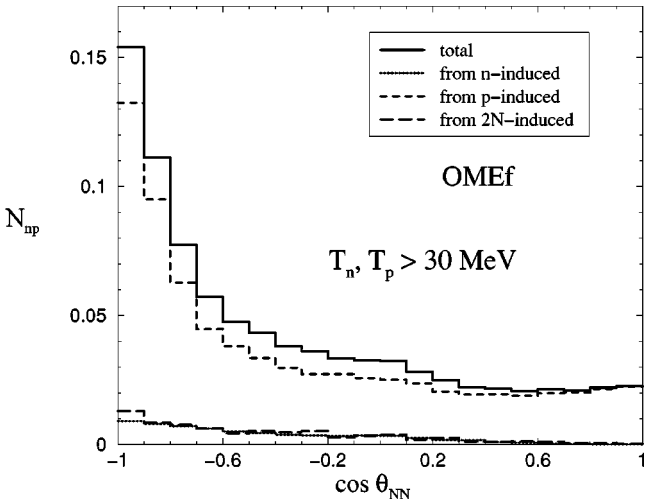

FIG. 9. Opening angle distributions of *np* pairs emitted in the nonmesonic decay of $^{12}_{\Lambda}$C. The total spectrum N_{np} (normalized *per nonmesonic weak decay*) has been decomposed in its components $N_{np}^{\Lambda n\to nn}$, $N_{np}^{\Lambda p\to np}$, and $N_{np}^{\Lambda np\to nnp}$ according to Eqs. (14) and (15).

In Fig. 9 we show the *np* pair opening angle distribution in the case of $^{12}_{\Lambda}$C. The total spectrum N_{np} has been decomposed into the components $N_{np}^{\Lambda n\to nn}$, $N_{np}^{\Lambda p\to np}$, and $N_{np}^{\Lambda np\to nnp}$. A nucleon energy threshold of 30 MeV has been used in the calculation. Figure 10 corresponds to the kinetic energy correlation of *np* pairs: it is again for $^{12}_{\Lambda}$C and $T_N^{\rm th}=30$ MeV, but

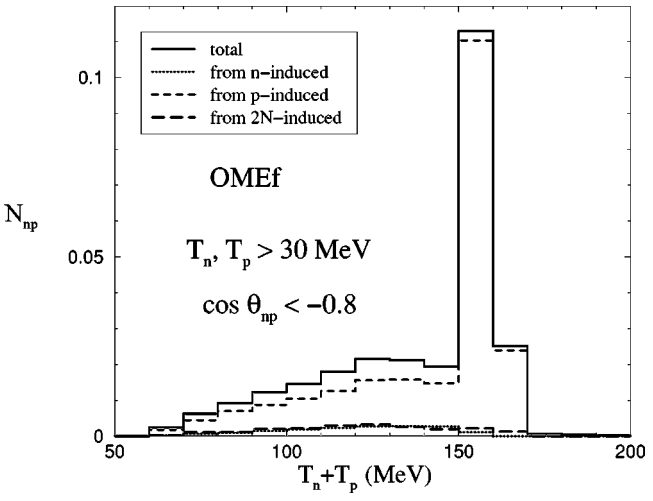

FIG. 10. Kinetic energy correlations of *np* pairs emitted in the nonmesonic decay of $^{12}_{\Lambda}$C at $\cos\theta_{np} \leqslant -0.8$. The total spectrum N_{np} (normalized per nonmesonic weak decay) has been decomposed in its components $N_{np}^{\Lambda n\to nn}$, $N_{np}^{\Lambda p\to np}$, and $N_{np}^{\Lambda np\to nnp}$ according to Eqs. (14) and (15).

TABLE IV. Predictions for the ratio $R_2 \equiv N_{nn}/N_{np}$ for ${}^{5}_{\Lambda}$He and ${}^{12}_{\Lambda}$C. An energy thresholds $T_N^{\rm th}$ of 30 MeV and two pair opening angle regions have been considered. The (preliminary) datum is from KEK-E462 [27].

	${}^{5}_{\Lambda}$He		${}^{12}_{\Lambda}$C	
	cos $\theta_{NN} \leqslant -0.8$	all θ_{NN}	cos $\theta_{NN} \leqslant -0.8$	all θ_{NN}
OPE	0.25	0.26	0.24	0.29
OMEa	0.51	0.45	0.39	0.37
OMEf	0.61	0.54	0.43	0.39
EXP	0.44 ± 0.11			

now only back-to-back angles (cos $\theta_{np} \leqslant -0.8$) have been taken into account. We note how both the *n*-induced and the two-nucleon induced decay processes give very small contributions to the total distributions in Figs. 9 and 10. Nevertheless, these decay processes could produce non-negligible interference terms. To minimize this effect, one could consider, for instance, not only back-to-back angles but also nucleon kinetic energies in the interval 150–170 MeV, for which we predict $I_{np}=0.18$. Again, smaller values of I_{np} have been obtained for ${}^{5}_{\Lambda}$He.

In Table IV the ratio N_{nn}/N_{np} predicted by the OPE, OMEa, and OMEf models for ${}^{5}_{\Lambda}$He and ${}^{12}_{\Lambda}$C is given for two opening angle intervals and for a nucleon energy threshold of 30 MeV. The results of the OMEa and OMEf models are in reasonable agreement with the preliminary KEK-E462 datum for ${}^{5}_{\Lambda}$He [27].

This datum ($N_{nn}/N_{np}=0.44\pm0.11$), which corresponds to an energy threshold of 30 MeV and cos $\theta_{np} \leqslant -0.8$, can be fitted by using the six weak interaction model independent quantities $N_{nn}^{1\rm Bn}$, $N_{nn}^{1\rm Bp}$, $N_{nn}^{2\rm B}$, $N_{np}^{1\rm Bn}$, $N_{np}^{1\rm Bp}$, and $N_{np}^{2\rm B}$ entering Eqs. (14) and (15) and quoted in Table V. This can be achieved through the following relation:

$$\frac{N_{nn}}{N_{np}} = \frac{\left(N_{nn}^{1\rm Bn} + N_{nn}^{2\rm B}\frac{\Gamma_2}{\Gamma_1}\right)\frac{\Gamma_n}{\Gamma_p} + N_{nn}^{1\rm Bp} + N_{nn}^{2\rm B}\frac{\Gamma_2}{\Gamma_1}}{\left(N_{np}^{1\rm Bn} + N_{np}^{2\rm B}\frac{\Gamma_2}{\Gamma_1}\right)\frac{\Gamma_n}{\Gamma_p} + N_{np}^{1\rm Bp} + N_{np}^{2\rm B}\frac{\Gamma_2}{\Gamma_1}}, \qquad (16)$$

using Γ_n/Γ_p and Γ_2/Γ_1 as fitting parameters.

TABLE V. Predictions for the weak interaction model independent quantities $N_{NN}^{1\rm Bn}$, $N_{NN}^{1\rm Bp}$, and $N_{NN}^{2\rm B}$ (integrated over all angles and for energies $T_N \geqslant 30$ MeV) of Eqs. (14) and (15) for ${}^{5}_{\Lambda}$He and ${}^{12}_{\Lambda}$C. The numbers in parentheses correspond to the angular region with cos $\theta_{NN} \leqslant -0.8$.

	$N_{nn}^{1\rm Bn}$	$N_{nn}^{1\rm Bp}$	$N_{nn}^{2\rm B}$
${}^{5}_{\Lambda}$He	0.84(0.53)	0.10(0.02)	0.54(0.34)
${}^{12}_{\Lambda}$C	0.56(0.30)	0.27(0.05)	0.30(0.12)
	$N_{np}^{1\rm Bn}$	$N_{np}^{1\rm Bp}$	$N_{np}^{2\rm B}$
${}^{5}_{\Lambda}$He	0.20(0.05)	0.98(0.49)	0.55(0.22)
${}^{12}_{\Lambda}$C	0.33(0.08)	1.22(0.38)	0.38(0.11)

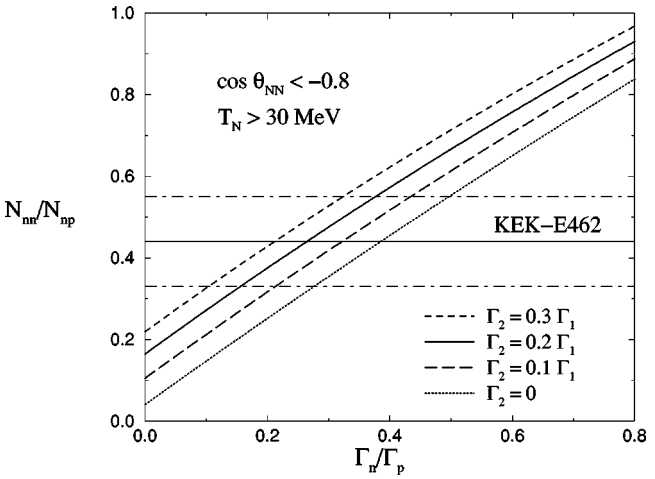

FIG. 11. Dependence of the ratio N_{nn}/N_{np} on Γ_n/Γ_p and Γ_2/Γ_1 for ${}^{5}_{\Lambda}$He. The results correspond to a nucleon energy threshold of 30 MeV and the angular restriction cos $\theta_{NN} \leqslant -0.8$. The horizontal lines show the preliminary KEK-E462 datum of Ref. [27].

In Fig. 11 (Fig. 12) we report the dependence of N_{nn}/N_{np} for ${}^{5}_{\Lambda}$He(${}^{12}_{\Lambda}$C) on the ratio Γ_n/Γ_p for four different values of Γ_2/Γ_1. Both figures correspond to the case with a nucleon energy threshold of 30 MeV and the angular restriction cos $\theta_{NN} \leqslant -0.8$. For a given value of Γ_2/Γ_1, Figs. 11 and 12 permit an immediate determination of Γ_n/Γ_p by a direct comparison with data for the observable N_{nn}/N_{np}.

By using the ${}^{5}_{\Lambda}$He datum $N_{nn}/N_{np}=0.44\pm0.11$ and assuming $\Gamma_2=0$, from Eq. (16) we obtain the following fitted ratio

$$\frac{\Gamma_n}{\Gamma_p}\left({}^{5}_{\Lambda}\mathrm{He}\right) = 0.39 \pm 0.11. \qquad (17)$$

By employing the value $\Gamma_2/\Gamma_1=0.2$ (i.e., the one obtained with the model of Ref. [12] and used in our calculations), a 34% reduction of the ratio is predicted

$$\frac{\Gamma_n}{\Gamma_p}\left({}^{5}_{\Lambda}\mathrm{He}\right) = 0.26 \pm 0.11. \qquad (18)$$

These values of Γ_n/Γ_p are rather small if compared with previous determinations [20] (0.93 ± 0.55) [28] (1.97 ± 0.67)

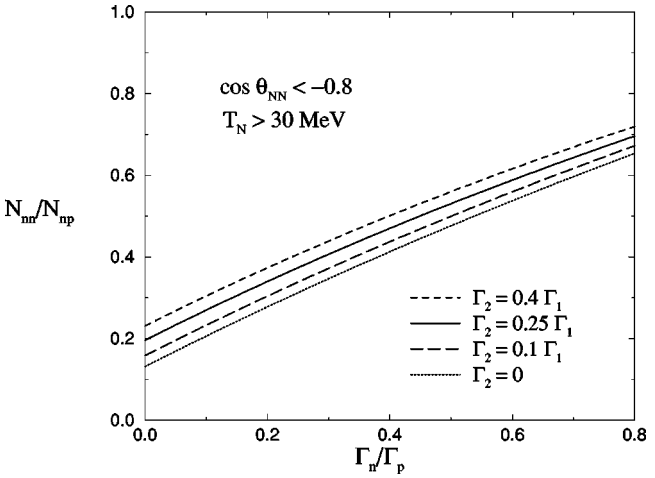

FIG. 12. Same as in Fig. 11 for ${}^{12}_{\Lambda}$C.

from single-nucleon energy spectra analyses. On the contrary, the ratios of Eqs. (17) and (18) are in agreement with the pure theoretical predictions of Refs. [6,7,14]. Since in Eq. (16) interferences are neglected, in our opinion this result provides an indirect but clear indication for a moderate contribution of such interference effects in double-coincidence spectra. To derive numerical constraints on these interferences, Eq. (16) should be modified using relations such as Eq. (9) for N_{nn} and N_{np}, which introduce new fitting parameters (six phases —three entering N_{nn} and other three for N_{np}—when the two-nucleon induced decay mechanism is included) in addition to Γ_n/Γ_p and Γ_2/Γ_1.

Forthcoming coincidence data from KEK and FINUDA could be directly compared with the results discussed in this paper and will permit to achieve new determinations of the Γ_n/Γ_p ratio and to establish the first constraints on Γ_2/Γ_1 and the interference effect.

VI. CONCLUSIONS

In this work we have presented a calculation of single and double-coincidence observables for the nucleons emitted in the nonmesonic weak decay of Λ hypernuclei. This has been possible by supplementing our OME weak interaction models with FSI through an intranuclear cascade calculation.

The predictions obtained with the OMEf model are in reasonable agreement with preliminary KEK-E462 data for the ratio N_n/N_p in ${}^{5}_{\Lambda}$He. Accordingly, the ratio Γ_n/Γ_p for ${}^{5}_{\Lambda}$He should be close to the value of 0.46 predicted by the OMEf model.

The results of the OMEa and OMEf calculations are also in reasonable agreement with preliminary KEK-E462 data for the ratio N_{nn}/N_{np} in ${}^{5}_{\Lambda}$He.

We also perform a weak interaction model independent analysis in which Γ_n/Γ_p and Γ_2/Γ_1 are considered as free parameters: the KEK ${}^{5}_{\Lambda}$He datum $N_{nn}/N_{np}=0.44\pm0.11$ is reproduced if $\Gamma_n/\Gamma_p=0.39\pm0.11$ and $\Gamma_2=0$ or $\Gamma_n/\Gamma_p=0.26\pm0.11$ and $\Gamma_2/\Gamma_1=0.2$.

The extension of the present study to triple-nucleon coincidence is of interest both for the determination of Γ_n/Γ_p and to disentangle the effects of one- and two-nucleon induced decay channels.

The values of Γ_n/Γ_p we obtain by fitting KEK coincidence data for ${}^{5}_{\Lambda}$He are in agreement with other recent theoretical evaluations. However, they are rather small if compared with the results of previous analyses from single-nucleon energy spectra. Actually, all the previous experimental analyses of single-nucleon spectra [19–22,28,37], supplemented in some cases by intranuclear cascade calculations, derived Γ_n/Γ_p values in disagreement with pure theoretical predictions. In our opinion, the fact that our calculations reproduce coincidence data for values of Γ_n/Γ_p as small as 0.3–0.4 could signal the existence of non-negligible interference effects between the *n*- and *p*-induced channels in those old single-nucleon data.

In conclusion, although further (theoretical and experimental) confirmation is needed, we think that our investigation proves how the study of nucleon coincidence observables can offer a promising possibility to solve the longstanding puzzle on the Γ_n/Γ_p ratio.

ACKNOWLEDGMENTS

This work was partly supported by EURIDICE HPRN-CT-2002-00311, by the DGICYT BFM2002-01868, by the Generalitat de Catalunya SGR2001-64, and by INFN. Discussions with O. Hashimoto, H. Outa, and Y. Sato are acknowledged.

[1] W. M. Alberico and G. Garbarino, Phys. Rep. **369**, 1 (2002).
[2] E. Oset and A. Ramos, Prog. Part. Nucl. Phys. **41**, 191 (1998).
[3] J. F. Dubach, G. B. Feldman, and B. R. Holstein, Ann. Phys. (N.Y.) **249**, 146 (1996).
[4] A. Parreño, A. Ramos, and C. Bennhold, Phys. Rev. C **56**, 339 (1997).
[5] D. Jido, E. Oset, and J. E. Palomar, Nucl. Phys. **A694**, 525 (2001).
[6] A. Parreño and A. Ramos, Phys. Rev. C **65**, 015204 (2002).
[7] K. Itonaga, T. Ueda, and T. Motoba, Phys. Rev. C **65**, 034617 (2002).
[8] A. Parreño, A. Ramos, C. Bennhold, and K. Maltman, Phys. Lett. B **435**, 1 (1998).
[9] W. M. Alberico and G. Garbarino, Phys. Lett. B **486**, 362 (2000).
[10] W. M. Alberico, A. De Pace, M. Ericson, and A. Molinari, Phys. Lett. B **256**, 134 (1991).
[11] A. Ramos, E. Oset, and L. L. Salcedo, Phys. Rev. C **50**, 2314 (1994).
[12] W. M. Alberico, A. De Pace, G. Garbarino, and A. Ramos, Phys. Rev. C **61**, 044314 (2000).
[13] W. M. Alberico, A. De Pace, G. Garbarino, and R. Cenni, Nucl. Phys. **A668**, 113 (2000).
[14] K. Sasaki, T. Inoue, and M. Oka, Nucl. Phys. **A669**, 331 (2000); **A678**, 455(E) (2000).
[15] K. Sasaki, T. Inoue, and M. Oka, Nucl. Phys. **A707**, 477 (2002).
[16] A. Parreño, C. Bennhold, and B. R. Holstein, nucl-th/0308074.
[17] A. Ramos, M. J. Vicente-Vacas, and E. Oset, Phys. Rev. C **55**, 735 (1997).
[18] A. Ramos, M. J. Vicente-Vacas, and E. Oset, Phys. Rev. C **66**, 039903(E) (2002).
[19] A. Montwill *et al.*, Nucl. Phys. **A234**, 413 (1974).
[20] J. J. Szymanski *et al.*, Phys. Rev. C **43**, 849 (1991).
[21] O. Hashimoto *et al.*, Phys. Rev. Lett. **88**, 042503 (2002). Since this paper used single-nucleon spectra from Ref. [17], the fits presented for Γ_n/Γ_p should be corrected (and have actually been corrected, in Ref. [22]) for the error explained in the Introduction. For ${}^{12}_{\Lambda}$C, the corrected ratio is 0.87 ± 0.23 whereas the uncorrected one is $1.17^{+0.22}_{-0.19}$.
[22] Y. Sato *et al.*, Phys. Rev. C (submitted).
[23] H. Outa *et al.*, KEK Report No. KEK–PS E462, 2000.

[24] A. Feliciello, Nucl. Phys. **A691**, 170c (2001); P. Gianotti, *ibid.* **A691**, 483c (2001).
[25] R. L. Gill, Nucl. Phys. **A691**, 180c (2001).
[26] G. Garbarino, A. Parreño, A. Ramos, Phys. Rev. Lett. **91**, 112501 (2003).
[27] H. Outa, Eighth International Conference on Hypernuclear and Strange Particle Physics (HYP2003), JLab, Newport News, Virginia [Nucl. Phys. A (to be published)].
[28] H. Noumi *et al.*, in *Proceedings of the IV International Symposium on Weak and Electromagnetic Interactions in Nuclei*, edited by H. Ejiri, T. Kishimoto, and T. Sato (World Scientific, Singapore, 1995), p. 550.
[29] J. Golak, K. Miyagawa, H. Kamada, H. Witala, W. Glockle, A. Parreño, A. Ramos, and C. Bennhold, Phys. Rev. C **55**, 2196 (1997); **56**, 2892(E) (1997).
[30] V. G. J. Stoks and T. A. Rijken, Phys. Rev. C **59**, 3009 (1999).
[31] J. Cugnon, D. L. Hôte and J. Vandermeulen, Nucl. Instrum. Methods Phys. Res. B **111**, 215 (1996).
[32] H. Kamada, W. Glockle, J. Golak and C. Elster, Phys. Rev. C **66**, 044010 (2002); J. Kuros-Zolnierczuk, H. Witala, J. Golak, H. Kamada, A. Nogga, R. Skibinski, and W. Glockle, *ibid.* **66**, 024003 (2002); **66**, 024004 (2002).
[33] J. Golak, H. Kamada, K. Miyagawa, H. Witala and W. Glockle, Phys. Rev. Lett. **83**, 3142 (1999).
[34] J. H. Kim *et al.*, Phys. Rev. C **68**, 065201 (2003). See also H. Bhang *et al.*, Nucl. Phys. **A691**, 156c (2001).
[35] H. Outa *et al.*, Nucl. Phys. **A670**, 281c (2000).
[36] H. Bhang, Eighth International Conference on Hypernuclear and Strange Particle Physics (HYP2003), JLab, Newport News, Virginia [Nucl. Phys. A (to be published)].
[37] H. Noumi *et al.*, Phys. Rev. C **52**, 2936 (1995).